an FVO strain and is R3-chloroquine resistant; no gametocytes are produced in culture. NF 54 is an Amsterdam airport strain, isolated in August 1979; it is a gametocyte producer (used routinely in Nymegen and elsewhere for mosquito infection) and is chloroquine-sensitive. NF 114 was isolated in July 1984 from a Dutch patient returning from West Java, Indonesia; it produces gametocytes and is chloroquine-resistant. Brazil strain isolate IMTM 22 (a gift from R. S. Nussenzweig) is a gametocyte producer and is chloroquine-sensitive.
9. M. Goman *et al.*, *Mol. Biochem. Parasitol.* **5**, 391 (1982).
10. Y. Pollack *et al.*, *Nucleic Acids Res.* **10**, 539 (1982).
11. G. H. Beale, A. Carter, D. Walliker, in *Rodent Malaria*, R. Killick-Kendrick and W. Peters, Eds. (Academic Press, London, 1978), pp. 213–244.
12. G. Langsley *et al.*, *Nucleic Acids Res.* **11**, 8703 (1983).
13. M. Koenen *et al.*, *Nature (London)* **311**, 382 (1984).
14. G. Langsley *et al.*, *Nucleic Acids Res.*, in press.
15. L. H. T. Van der Ploeg and A. W. C. A. Cornelissen, *Phil. Trans. R. Soc. Lond. B. Biol. Sci.*, in press.
16. L. H. T. Van der Ploeg and S. H. Giannini, unpublished data.
17. Preparations of parasites from erythrocyte cultures or from saponin-lysed samples gave identical results. Ten-milliliter samples of erythrocyte suspension cultures (10 ml; 3×10^9 erythrocytes) (*18, 20*) gave 10 percent infected cells. The parasite population resulting from these cultures consisted of ring forms (80 percent) and a variable number of trophozoites and schizonts (approximately 10 percent each). Parasites were put in agarose blocks at a cell density of 3×10^8 cells per milliliter and were lysed as described (*3*). The NF 7/7 gametocytes and gametes were prepared by a modification of a method described previously (*18–20*). The gametocyte suspension was contaminated (5 to 10 percent) with schizonts; the macrogamete fraction, although free of schizonts, was contaminated with residual bodies of microgametes (less than 5 percent). The presence of some zygotes in the latter preparation could not be excluded. The cells were lysed and the agarose blocks were inserted in the slots of a 1 percent agarose gel (*2–5*).
18. *Plasmodium falciparum* asexual and sexual stages were produced in 10-ml suspension culture systems. Medium change was automated and occurred twice daily (*19*).
19. T. Ponnudurai *et al.*, in preparation.
20. A. N. Vermeulen *et al.*, *Trans. R. Soc. Trop. Med. Hyg.* **77**, 753 (1983).
21. We thank A. Cornelissen, S. Parangi, T. Lensen, and P. van de Ven for help in the experiments; O. Mercereau-Puijalon for support and discussion; D. Walliker, M. Goman, and M. Konen for gifts of strains; and D. Tse, R. Rothstein, and C. Cantor for their critical reading of the manuscript. This work was supported in part by a grant from the John D. and Catherine T. MacArthur Foundation and by a Medical Research Council–Institut National de Science et Recherche Medicale fellowship to G.L.

27 March 1985; accepted 20 May 1985

Picosecond Time–Resolved Resonance Raman Studies of Hemoglobin: Implications for Reactivity

Abstract. *Picosecond time–resolved Raman spectra of hemoglobin generated with blue pulses (20 to 30 picoseconds) that were resonant with the Soret band and of sufficient intensity to completely photodissociate the starting liganded sample are reported. For both R- and T-state liganded hemoglobins, the peak frequencies in the spectrum of the deoxy transient were the same at approximately 25 picoseconds as those observed at 10 nanoseconds subsequent to photodissociation. In particular, the large R-T differences in the frequency of the stretching mode for the iron-proximal histidine bond ($\nu_{Fe\text{-}His}$) detected in previously reported nanosecond-resolved spectra were also evident in the picosecond-resolved spectra. The implications of this finding with respect to the distribution of strain energy in the liganded protein and the origin of the time course for geminate recombination are discussed. On the basis of these results, a microscopic model is proposed in which delocalization of strain energy is strongly coupled to the coordinate of the iron. The model is used to explain the origin of the R-T differences in the rates of ligand dissociation.*

E. W. Findsen*
J. M. Friedman
AT&T Bell Laboratories, Murray Hill, New Jersey 07974
M. R. Ondrias
Department of Chemistry, University of New Mexico, Albuquerque 87106
S. R. Simon
Department of Biochemistry, State University of New York, Stony Brook 11794

*Permanent address: Department of Chemistry, University of New Mexico, Albuquerque 87106.

Although efforts to determine the functional and the structural properties of proteins have met with great success, a clear picture of how energy is stored within a protein and utilized for function is still not available. As a case in point, the static structure and functional properties of hemoglobin (Hb) are exceedingly well characterized (*1, 2*), yet even for this well-studied system a detailed microscopic account of the relation between structure and function is lacking. Part of the problem is that, although high-resolution x-ray crystallographic techniques provide detailed information about equilibrium structures, they cannot be readily used to probe the transient structures that link the initial and final functional states of a protein.

The equilibrium structures of ligand-free and ligand-bound Hb are well characterized (*1, 3*). In going from the ligand-free to ligand-bound protein, the local tertiary structure about the binding site responds to the change in both the quaternary structure (low-affinity T state → high-affinity R state) and the state of ligation at the heme (deoxy → liganded). To fully explore how protein structure controls the ligand-binding properties of the heme, it is necessary to determine how the local tertiary structure responds to functionally important perturbations (change in quaternary structure, ligand dissociation) and to establish correlations between specific structural features associated with the tertiary structures and parameters of ligand binding. One approach has been to study the ligand dissociation by rapidly photodissociating the ligand-bound protein and monitoring the subsequent dynamics of ligand and protein. Initial microsecond studies (*4*) focused on the bimolecular rebinding process, in which a ligand from the solvent rebinds to a heme surrounded by a protein that has partially relaxed from its initial structure. More recently, nanosecond (*5–7*) and picosecond (*8*) studies revealed much faster geminate (cage) rebinding processes. Transient Raman (*9–11*) and absorption (*7, 12*) studies have also probed the structural relaxation occurring on nanosecond and longer time scales. However, even the nanosecond Raman measurements (*13–16*) do not bridge the temporal and structural gap to the initial well-characterized structure of the liganded protein. We report here high-quality picosecond transient Raman spectra of photodissociated liganded Hb generated with blue, picosecond pulses of sufficient intensity to photolyze a sizable fraction of the starting material. The structural information in these spectra provides the link between the structure of the starting liganded Hb and the abundant functional and structural data obtained on the nanosecond and microsecond transients.

Single blue, picosecond pulses (435 nm, 10 mW, 10 Hz) were used to generate the low-frequency Raman spectra of the transient species that occurs within 20 to 30 psec after the photolysis of various R- and T-state liganded Hb's. Previous picosecond Raman investigations (*17*) in which low-intensity yellow pulses were used showed only that the transient form occurring within 30 psec of photolyzing COHbA (HbA, adult hemoglobin) had a high-frequency spectrum characteristic of a deoxy heme. Figure 1 shows a segment of the low-frequency portion of the picosecond Raman spectra from several different photodissociated COHb's. In each instance the frequencies of the spectral peaks at ~25 psec are identical to those of the corresponding deoxy transient at 10 nsec after photolysis. Substantial photolysis of the illuminated sample was achieved, as evidenced by the near-absence of the

heme ν_4 mode characteristic of the liganded species (at ~1376 cm^{-1}) (Fig. 2). Compared to the 10-nsec spectra, the spectral width associated with $\nu_{Fe\text{-}His}$ but not the other peaks appears broadened in the picosecond spectrum. The photolyzed O_2HbA sample gave a lower signal-to-noise deoxy spectrum because of a reduced yield for photolysis. The O_2HbA spectrum did not appear substantially different from that of the corresponding photolyzed COHbA sample. Table 1 summarizes the values of $\nu_{Fe\text{-}His}$ in the picosecond and nanosecond transients.

This study shows that, within 25 psec of photolysis, the shifted frequencies of $\nu_{Fe\text{-}His}$ for the transient forms derived from both the "strained" liganded R state (COHbA at *p*H 6 with inositol hexaphosphoric acid) and the liganded T state are already fully developed. The rate at which these frequency differences appear and develop is of fundamental importance for the analysis of geminate recombination. Geminate recombination in Hb has been observed to occur with an ~100-nsec time constant for both O_2 (*6*) and CO (*5–7*). Picosecond studies have revealed that 40 to 50 percent of the photodissociated oxygens recombine within 200 psec subsequent to photolysis for O_2HbA (*8*), whereas only a small fraction of the photodissociated CO recombines on this time scale (*8, 18–20*). More recent studies show that the subnanosecond rebinding of O_2 is responsive to the conformation of the protein (*20*). The changes in the yield of the subnanosecond geminate process are correlated with $\nu_{Fe\text{-}His}$ in the deoxy transient occurring within 10 nsec of photolysis (*12*). A decrease in $\nu_{Fe\text{-}His}$ (at 10 nsec) such as occurs in going from a photolyzed R-state to a photolyzed T-state liganded Hb is associated with a substantial decrease in the yield of subnanosecond rebinding for the oxygen ligand. The observation of the fully developed R- and T-state deoxy transient within 25 psec of photolysis indicates that the time dependence of the subnanosecond geminate rebinding is not due to a structural evolution at or about the heme. Instead, as previously suggested (*21*), it seems likely that the observed rate at ambient temperature is due to competition between the rates associated with the diffusion of the ligand away from the iron into the bulk protein and the heme-associated potential energy barrier for rebinding. Protein control of this barrier has been linked to the induced changes in the proximal histidine that give rise to the variation in $\nu_{Fe\text{-}His}$ (*10, 14–16*). Conditions that decrease

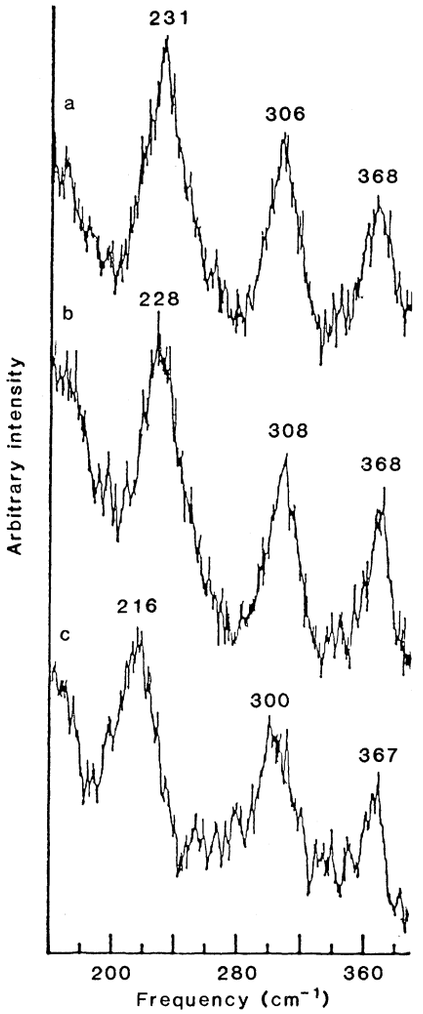

Fig. 1. Low-frequency portion of the resonance Raman spectra of the deoxy transients occurring within 25 ± 5 psec of the photodissociation of several different COHb's: (a) ~100 μ*M* HbA in 0.1*M* tris (*p*H 8.2), (b) ~100 μ*M* HbA in 0.1*M* bis-tris (*p*H 6.0) + 2 m*M* IHP, and (c) ~100 μ*M* carp Hb in 0.1*M* bis-tris (*p*H 6.0) + 3 m*M* IHP. The frequency of the peak occurring on the left (216 to 231 cm^{-1}) is $\nu_{Fe\text{-}His}$, the frequency of the iron-proximal histidine stretching mode. The spectra were generated with pulses from an active-passive mode-locked Nd:YAG laser (Quantel YG 471C) operating at 10 Hz. Blue pulses (435 nm; average power, 15 to 20 mW) were generated by passing the single 30-psec-long second harmonic (532 nm) through a hydrogen cell (300 psi). The blue pulses, resulting from the first anti-Stokes Raman transition, were determined to be between 20- and 30-psec long on the basis of rise time measurements of a known subpicosecond transient absorption change with a slowly scanned optical delay line. The blue pulses were loosely focused (250-mm focal-length lens) onto a flowing stream of recirculated but coarsely filtered Hb solution. The 90° scattered radiation was collected, dispersed, and analyzed (*8*). The spectra are the result of two or three scans with a signal averager coupled to a spectrometer operating at 10 pulses per 0.1 cm. The blue pulses were of sufficient intensity to substantially photolyze the illuminated sample volume, as determined by the ratio of the intense 1355/1375 cm^{-1} peaks. Absorption measurements before and after each run established the integrity of the liganded Hb samples.

$\nu_{Fe\text{-}His}$ decrease the yield for the subnanosecond geminate rebinding. The appearance at 25 psec of the R-T difference in $\nu_{Fe\text{-}His}$ suggests that this decrease results from a higher average barrier for recombination, which increases the probability that the ligand will diffuse away from the heme instead of rebinding.

The observation that the frequencies in the Raman spectra of transient deoxy Hb's are stable from within 25 psec of photolysis until the onset at tens of nanoseconds of the *p*H-dependent relaxation of the tertiary structure (*10*) suggests that these early frequencies reflect the influence of the unrelaxed structure of the parent liganded protein on the deoxy heme. The substantial R-T differences observed in the spectra of the transients imply that the spectra of the parent liganded proteins should exhibit corresponding R-T differences. All vibrational measurements indicate that they do not (*22–27*). There are essentially no R-T differences in the Raman spectra of O_2Hb (Kansas) (*22*), COHb (Kansas) (*23, 25*), COHb (carp) (*25*) and COHb (*Acrochordus javanicus*) (*26*). The only differences observed are ≤0.8 cm^{-1} in ν_1 at ~1375 cm^{-1}. Most significant is the observation (*22–27*) that there are no R-T differences in the stretching frequency of the iron ligand (CO, O_2, NO) for the six-coordinate Fe^{2+} heme despite the large R-T differences in $\nu_{Fe\text{-}His}$ in the corresponding photolyzed Hb's (*13–16, 20*). Studies of model porphyrins show that electronic and steric differences on the proximal side are transmitted to the distal side (*28*). Although $\nu_{Fe\text{-}His}$ has not been identified in the Raman spectra of liganded Hb's the above findings, in conjunction with the studies of model porphyrins, have led to the conclusion (*25, 27*) that anticipated R-T differences in strain energy are not localized at the heme and that the iron-proximal environment is essentially the same for R- and T-state COHb. This is further supported by the recent finding that both the distal and proximal iron-ligand distances are essentially identical in R and T forms of COHb (carp) (*29*).

These conclusions, which are consistent with the description of the distributed energy of cooperative binding in Hb (*30*), raise several fundamental questions. Given that there is no evidence for a picosecond change in protein tertiary structure, how do we account for the presence and absence of R-T differences at the iron for the transients and liganded Hb's, respectively? And how do we account for the large R-T difference in the intrinsic iron-ligand dissociation rate (*7,*

20, 31) if there is little or no R-T difference in the equilibrium geometry about the iron?

Our finding that the R-T differences materialize at the heme within 25 psec of dissociation indicates that ligand-induced delocalization of the strain energy cannot be distributed over many delocalized degrees of freedom. Instead, it suggests a tight coupling between changes at the heme associated with deligation and some localized region in the protein. The most obvious and likely change at the heme is the movement of the iron in and out of the heme plane upon ligand binding and dissociation, respectively. Femtosecond transient absorption studies (*19*) and theoretical calculations (*32*) show that, upon dissociation, the iron moves from a planar to an out-of-plane geometry within a fraction of a picosecond. Our Raman results show that within 25 psec of dissociation the heme has the characteristic of a nonplanar, high-spin, five-coordinate Fe^{2+} system. Under these conditions, $\nu_{Fe\text{-}His}$ is modulated by those elements of the tertiary structure that are linked to those which define and stabilize the quaternary structure (*11, 13–16*). From a theoretical analysis, Karplus and co-workers (*33*) suggested that an "allosteric core" composed of the heme, proximal histidine, part of the F helix, and the FG corner (an essential component of the α_1-β_2 interface) plays an essential role in the mechanism of cooperative ligand binding. This allosteric core also satisfies the requirements for a structural unit that links the heme-histidine unit with the quaternary state.

The allosteric core provides a framework for analyzing the relation between protein structure and control of ligand binding at the level of the heme. A direct connection between the allosteric core and the Raman data is provided by the suggestion that the variation in $\nu_{Fe\text{-}His}$ for the deoxy hemes originates from a change in the tilt of the proximal histidine (in its own plane) with respect to the plane of the heme (*13–16*). The lower the value of $\nu_{Fe\text{-}His}$, the greater the tilt. Karplus and co-workers (*33*) identified such tilting in x-ray structures and pointed out the potential significance of the tilt in the mechanism of cooperative binding. For the unliganded heme, the "relevant" configuration of the heme-histidine unit is determined by the orientation of the heme in the heme pocket and the pull on the proximal histidine by the F helix. The orientation of the heme and the angle of rotation of the histidine are determined by interactions with the surrounding amino acids (*33*). The pull on the histidine, which determines the tilt,

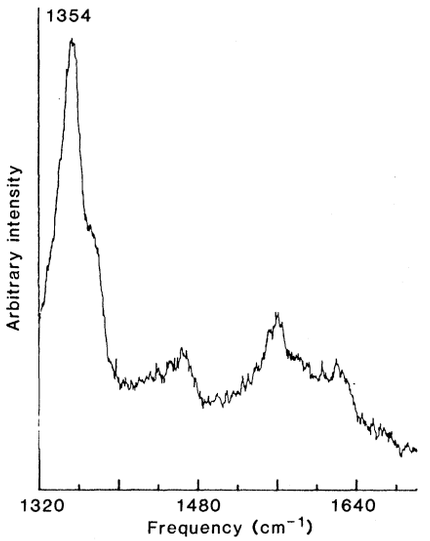

Fig. 2. High-frequency portion of the resonance Raman spectrum of the deoxy transient of HbA obtained under the same conditions as in Fig. 1a.

is generated through the F helix by the α_1-β_2 interface (Fig. 3). The magnitude of the pull is determined by the geometry of the α_1-β_2 interface. It is strongest for the T state and weakest for the R state, with species-specific variations for each quaternary state. Solution conditions, such as *p*H and phosphate concentration, that affect the interface (the stability of the quaternary state) also affect the histidine through the above pathway. At the heme the pull of the interface is opposed by the repulsive interaction between the heme and the nearest carbon ($C_{\epsilon 1}$) of the histidine imidazole. This interaction favors an untilted geometry between the histidine and the heme. The repulsive force substantially increases upon moving the iron into the plane of the porphyrin (*33, 34*). Such movement occurs upon ligand binding. For both equilibrium and transient deoxy Hb's, the iron is out of the heme plane and the repulsive force is at a minimum. Under these conditions, in which the influence of the interface-generated pull at the heme is least opposed by the repulsive interactions, the tilted geometry will be most evident, as is indeed seen in the large and systematic distribution of $\nu_{Fe\text{-}His}$ values observed for stable and transient deoxy species (*13–16*). The lowest frequencies (the most tilted) are associated with the deoxy T-state species, whereas the highest frequencies (least tilted) are observed for deoxy transients generated from high-affinity liganded R-state species (such as photolyzed carboxy or oxy HbA at *p*H 8.5). Under these conditions of reduced repulsion, the R-T energy difference due to the heme-histidine interaction is at a minimum (Fig. 3c). Ligand binding causes the iron to move into the plane of the porphyrin; concomitantly the tilt-dependent heme-histidine repulsive force increases substantially. Because of the difference in the repulsive force, it will be energetically costly to move the

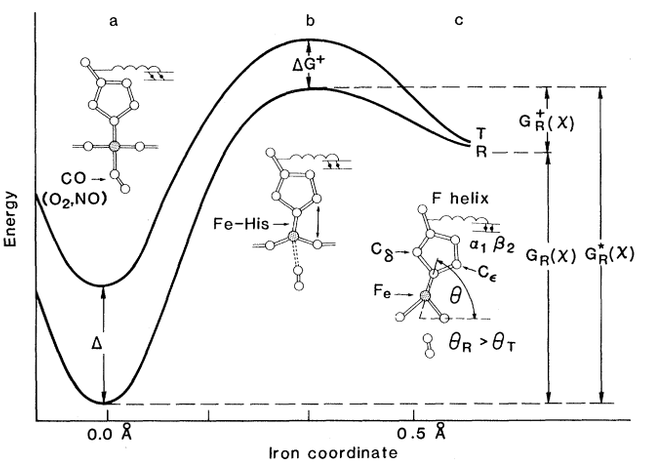

Fig. 3. Reaction coordinate diagram for R- and T-state liganded Hb showing the effect of proximal displacements of iron out of the heme plane. When the iron is in plane (a), the strong repulsive forces between the imidazole carbons and the pyrrole nitrogens maintain the proximal histidine in an upright orientation. As the iron undergoes a proximal displacement (b), the repulsive forces decrease. When the pull from the F helix (generated by the α_1-β_2 interface) exceeds the torque on the histidine from the decreasing repulsive force, the histidine will start to tilt. When the ligand-iron bond is finally ruptured (c) and the iron is substantially displaced from the heme plane, the histidine will initially have assumed the maximally tilted orientation consistent with the forces generated by the yet unrelaxed tertiary structure of the starting liganded protein. In the nonplanar deoxy hemes the repulsive forces are substantially reduced; consequently, the R-T energy differences due to the histidine tilt are much less for (c) relative to the more planar (a). The additional energy required to bring the iron in plane upon ligation for the tilted geometry gives rise to ΔG and ΔG^+. $G(\chi)$, $G^*(\chi)$, and $G^+(\chi)$ are the decrease in energy upon ligation, the spontaneous dissociation energy, and the height of the innermost energy barrier for geminate rebinding, respectively, for a given tertiary structure having the parallel reaction coordinate χ. As the tertiary structure relaxes after dissociation, χ and the above associated energies also change (*11*).

Table 1. Comparison of $\nu_{Fe\text{-}His}$ values for the deoxy transients occurring within 10 nsec and 25 psec of the photodissociation of several different R- and T-state COHb's. Relaxation of $\nu_{Fe\text{-}His}$ to values typical of equilibrium R- and T-state deoxy Hb's (222 ± 2 and 215 ± 1 cm^{-1}, respectively) occurs over hundreds of nanoseconds to tens of microseconds (*9–11*). The uncertainty in the peak frequencies represents the confidence level associated with the measurement. IHP, inositol hexaphosphoric acid.

Sample	*p*H	Fe-His frequency (cm^{-1})		Quaternary structure
		10 nsec	25 psec	
HbA	8.2	230 ± 1	231 ± 1	R
HbA + IHP	6.0	227 ± 1	228 ± 1	R
Hb (carp) + IHP	6.0	216 ± 1	216 ± 1	T
Hb (*A. javanicus*)* + IHP	6.0	220 ± 2	220 ± 2	T

*Hemoglobin from the highly aquatic Javan wart snake, which can be switched to the T state at *p*H 6.0 + IHP even when saturated with CO (*36*).

T-state iron into the heme plane by an amount ΔG (Fig. 3a). The increase in the repulsive force upon ligand binding generates a torque that strongly counters the pull of the F helix. The inability to spectroscopically detect R-T differences at the iron for carboxy and oxy Hb's (Fig. 3a) (*22–27*) suggests that the torque is adequate to overcome (straighten) the tilt of the histidine regardless of the geometry of the interface (that is, R or T). As the histidine straightens, the F helix is pulled. This pull counters the pull from the interface. Thus the F helix also provides a conduit through which local changes at the heme (ligation) are transmitted to the interface.

Although the effective environment at the iron is nearly the same for R and T for the planar geometry, structural differences exist in other regions of the allosteric core. The picosecond Raman spectra indicate that these differences are communicated to the iron within 25 psec. This communication must be coupled to structural or electronic events that occur subsequent to or concomitant with dissociation. As discussed earlier, the most obvious event is the displacement of the iron proximal to the heme plane. As the iron moves out of the heme plane, there is a reduction in the repulsive forces that favor the nontilted heme-histidine geometry of the in-plane configuration. With the diminution of this repulsive force and the associated torque upon the histidine, the differential pull of the R and T α_1-β_2 interfaces now becomes evident at the heme, but the magnitude of ΔG decreases greatly (Fig. 3c). The reappearance of the R-T differences within 25 psec after photodissociation is an indication that the shuttling and modulation of strain between the binding site and the α_1-β_2 interface is strongly linked to the position of the iron. This tight, springlike coupling between the iron coordinate and the interface via the F helix should be evident upon using picosecond ultraviolet resonance Raman measurements to probe the change in the interface at the "instant" of photodissociation.

Strong coupling in the allosteric core has a direct effect on the barrier height for dissociation. The curvature at the bottom of the potential well is nearly identical for both the R- and T-state liganded heme (*22–27*). However, the T-state minimum is displaced by an amount ΔG because of the extra energy required to go from a tilted nonplanar geometry to a nontilted planar geometry. The magnitude of ΔG is reduced, however, when the iron undergoes thermally induced fluctuations that move it proximal to the heme plane (Fig. 3). During such fluctuations the iron-ligand bond is stretched for both R- and T-state forms. Because of the reduction in the heme-histidine repulsive interactions and the proposed tight coupling between the iron and the F helix, the energy stored away from the heme for the planar geometry is reduced as the iron undergoes this proximal fluctuation. Therefore, to the extent that the transition state (Fig. 3b) for spontaneous dissociation has a configuration with a partially displaced iron, the R-T difference in the transition state energy, ΔG^+, will be less than ΔG. Thus the barrier height for spontaneous dissociation will be lower for the T-state species by an amount determined by the difference between ΔG and ΔG^+. As pointed out by Szabo (*35*), the nature of the transition state and hence ΔG^+ will depend on the ligand. Since ΔG is not ligand-dependent in the first approximation, the R-T difference in the intrinsic rate of dissociation (ΔG-ΔG^+) will be ligand-dependent as is observed (*31*).

In summary, we have obtained picosecond transient Raman data that establish tight new criteria for models of cooperative phemomena in hemoglobin. We incorporated several earlier concepts (*1, 2, 13–16, 27, 30, 33, 35*) into a model that is more detailed with respect to structure and dynamics. The essential assumptions on which this model is based are as follows:

1) The major determinant of the variation in the stretching frequency of the iron-proximal histidine linkage is the tilt angle θ (Fig. 3).

2) Angular strain, which is evident at the heme when the iron is out of plane (as in the deoxy heme), arises from an elastic coupling between the α_1-β_2 interface and the heme-histidine (F8) linkage through the F helix.

3) The angular strain is not apparent at the heme in the typical liganded complex because, when the iron is in plane, the increased repulsive force between the heme and the histidine determines the local geometry at the iron.

4) As a result of tight coupling among the elements of the allosteric core, the location and the magnitude of the stored strain energy are modulated by the static and dynamic properties of the iron coordinate.

References and Notes

1. M. F. Perutz, *Proc. R. Soc. London Ser. B* **208**, 135 (1980).
2. R. G. Shulman, J. J. Hopfield, S. Ogawa, *Q. Rev. Biophys.* **8**, 325 (1975).
3. J. M. Baldwin and C. Chothia, *J. Mol. Biol.* **129**, 175 (1979).
4. Q. H. Gibson, in *Hemoglobin and Oxygen Binding*, C. Ho, Ed. (Elsevier, New York, 1982), pp. 322–327.
5. D. A. Duddell, R. J. Morris, J. T. Richards, *J. Chem. Soc. Chem. Commun.* **1979**, 75 (1979); B. Alpert, S. El Moshni, L. Lindqvist, F. Tfibel, *Chem. Phys. Lett.* **64**, 11 (1979); J. M. Friedman and K. B. Lyons, *Nature (London)* **284**, 570 (1980).
6. D. A. Duddell, R. J. Morris, N. J. Muttcuman, J. T. Richards, *Photochem. Photobiol.* **31**, 479 (1980).
7. J. Hofrichter *et al.*, *Proc. Natl. Acad. Sci. U.S.A.* **80**, 2235 (1983).
8. D. A. Chernoff, R. M. Hochstrasser, A. W. Steele, *ibid.* **77**, 5606 (1980).
9. K. B. Lyons and J. M. Friedman, in *Hemoglobin and Oxygen Binding*, C. Ho, Ed. (Elsevier, New York, 1982), pp. 333–338; C. P. Stein and T. G. Turner, *J. Phys. Chem.* **86**, 168 (1981).
10. M. J. Irwin and G. H. Atkinson, *Nature (London)* **293**, 317 (1981).
11. T. W. Scott and J. M. Friedman, *J. Am. Chem. Soc.* **106**, 5677 (1984).
12. L. Lindqvist, El Mohsni, F. Tfibel, B. Alpert, *Nature (London)* **288**, 729 (1980).
13. J. M. Friedman, D. L. Rousseau, M. R. Ondrias, R. A. Stepnoski, *Science* **218**, 1244 (1982); T. W. Scott, J. M. Friedman, M. Ikeda-Saito, T. Yonetani, *FEBS Lett.* **158**, 68 (1983).
14. J. M. Friedman, R. A. Stepnoski, R. W. Noble, *FEBS Lett.* **146**, 278 (1982).
15. J. M. Friedman, in *Time-Resolved Vibrational Spectroscopy*, G. Atkinson, Ed. (Academic Press, New York, 1983), p. 307.
16. T. W. Scott *et al.*, *J. Biol. Chem.* **258**, 10,564 (1983).
17. J. Turner *et al.*, *Proc. Natl. Acad. Sci. U.S.A.* **78**, 1313 (1981).
18. J. A. Hutchinson, T. G. Taylor, L. J. J. Noe, *J. Am. Chem. Soc.* **104**, 3321 (1982).
19. J. L. Martin *et al.*, *Proc. Natl. Acad. Sci. U.S.A.* **80**, 173 (1983).
20. J. M. Friedman *et al.*, *Science*, in press.
21. W. Doster *et al.*, *Biochemistry* **21**, 4831 (1982); D. D. Dlott, H. Frauenfelder, B. Langer, H. Roder, E. E. Dilorio, *Proc. Natl. Acad. Sci. U.S.A.* **80**, 6239 (1983); H. Roder *et al.*, *ibid.*, in press.
22. K. Nagai, T. Kitagawa, H. Morimoto, *J. Mol. Biol.* **136**, 2271 (1980).
23. M. Tsubaki, R. B. Srivastava, N.-T. Yu, *Biochemistry* **21**, 1132 (1982).
24. M. Tsubaki and N.-T. Yu, *ibid.*, p. 1140.
25. D. L. Rousseau, S. L. Tan, M. R. Ondrias, S. Ogawa, *Biochemistry* **23**, 2857 (1984).

26. P. Argade, J. M. Friedman, D. L. Rousseau, unpublished results.
27. D. L. Rousseau and M. R. Ondrias, *Biophys. J.* **47**, 726 (1985).
28. E. A. Kerr, C. H. Mackin, N.-T. Yu, *Biochemistry* **22**, 4373 (1983); W. R. Scheidt, A. C. Briniger, E. B. Ferro, J. F. Kirner, *J. Am. Chem. Soc.* **99**, 7315 (1972).
29. M. Chance *et al.*, *Biophys. J.* **47**, 84a (1985).
30. S. Ogawa and R. G. Shulman, *J. Mol. Biol.* **70**, 315 (1972); J. J. Hopfield, *ibid.* **77**, 207 (1973).
31. R. J. Morris and Q. H. Gibson, *J. Biol. Chem.* **259**, 365 (1984).
32. E. R. Henry and W. A. Eaton, *Biophys. J.* **47**, 208a (1985); E. R. Henry, M. Levitt, A. W. A. Eaton, *Proc. Natl. Acad. Sci. U.S.A.* **82**, 2034 (1985).
33. B. R. Gelin and M. Karplus, *Proc. Natl. Acad. Sci. U.S.A.* **74**, 801 (1977); B. R. Gelin, A. W.-M. Lee, M. Karplus, *J. Mol. Biol.* **171**, 489 (1983).
34. B. D. Olafson and W. A. Goddard, *Proc. Natl. Acad. Sci. U.S.A.* **74**, 1315 (1979); W. A. Goddard and B. D. Olafson, in *Biochemical and Chemical Aspects of Oxygen*, W. Caughy, Ed. (Academic Press, New York, 1979), pp. 87–123; A. Warshel, *Proc. Natl. Acad. Sci. U.S.A.* **74**, 1789 (1977).
35. A. Szabo, *Proc. Natl. Acad. Sci. U.S.A.* **75**, 2108 (1978).
36. J. M. Friedman, S. R. Simon, T. W. Scott, *Copeia*, in press.
37. M.R.O. gratefully acknowledges the support of NIH (grants RO1 GM3333O-01 and DHHS 2-506 RR-8139) and the donors of the Petroleum Research Fund as administered by the American Chemical Society. J.M.F. gratefully acknowledges the helpful and insightful comments of M. Stavola and J. Tully. The carp Hb and Hb (Kempsey) were generously supplied by R. Noble and F. Bunn, respectively. J.M.F. thanks M. Chance for sharing his EXAFS results.

25 February 1985; accepted 5 June 1985

The Brain Connection:
The Corpus Callosum Is Larger in Left-Handers

Abstract. *The size of the midsagittal area of the human corpus callosum obtained from postmortem measurement varied with tested hand preference. The corpus callosum, the main fiber tract connecting the two cerebral hemispheres, was larger by about 0.75 square centimeter, or 11 percent, in left-handed and ambidextrous people than in those with consistent right-hand preference. The difference was present in both the anterior and posterior halves, but not in the region of the splenium itself. This callosal morphology, which varied with hand preference, may also be related to individual differences in the pattern of hemispheric functional specialization. The greater bihemispheric representation of cognitive functions in left- and mixed-handers may be associated with greater anatomical connection between the hemispheres. The naturally occurring regressive events in neurogenesis, such as neuronal cell death and axonal elimination, may be factors in the individual differences in brain morphology and in functional lateralization. Specifically, right-handers may be those with more extensive early elimination of neural components.*

SANDRA F. WITELSON
Departments of Psychiatry, Psychology, and *Neurosciences, McMaster University, Hamilton, Ontario L8N 3Z5, Canada*

Functional specialization of the cerebral hemispheres in the mediation of cognition in humans has been known for over a century (*1*) and extensively documented (*2, 3*), but its neurobiological basis is not known. Right-left asymmetry in the pattern of cortical sulci and gyri, particularly in the posterior opercular regions, was documented long ago (*4, 5*). Only recently, however, has some quantitative study been made of gross anatomical (*6*) and histological (*7*) asymmetry, and has the anatomical asymmetry been suggested to be a substrate of functional asymmetry. It remains to be established whether these anatomical asymmetries have biological significance for hemispheric functional specialization (*8*). One of the main obstacles to such study is that information is difficult to obtain for both anatomical and functional asymmetry in the same subjects (*9*). A general pattern of hemispheric specialization, in which linguistic-sequential and spatial tasks are more accurately processed in the left and right hemispheres, respectively, exists for most people, but the pattern may vary in both direction and degree (*3*). Different patterns of lateralization may be associated with such factors as brain damage, extreme deprivation, cognitive disorders (*10*), sex, and, most clearly, hand preference (*3*).

Hand preference is related, although imperfectly, to the pattern of hemispheric specialization. Left-handers as a group have greater bihemispheric representation of cognitive functions than do right-handers (*3*). As the main interhemispheric tract, the corpus callosum plays an important role in hemispheric integration and possibly in hemispheric specialization. As part of a larger study on the relation of neuroanatomical and neuropsychological measures in the same subjects (*11*), it was possible to study the anatomy of the corpus callosum in relation to hand preference, which was chosen as an index of functional lateralization. Almost no data are available relating postmortem neuroanatomical measures to indices of functional lateralization (*12*).

I now report that the size of the corpus callosum is correlated with the neuropsychological measure, hand preference. The midsagittal area of the corpus callosum was larger in the left-handed and ambidextrous than in the right-handed by 73 mm^2, or 11 percent. Such a difference could represent as many as 25 million fibers (*13*). This finding may have implications for the neuroanatomical basis of hemispheric specialization and for the early neurobiological precursors of hand preference. The gross variation in callosal size makes it a potential morphological marker for use with new brain imaging technology such as magnetic resonance imaging (MRI) for the study of hemispheric specialization in vivo in normal humans and in clinical populations suspect for atypical functional lateralization.

The 42 subjects studied (*14*) ranged in age from 25 to 65 years at the time of death. The handedness test, adapted from a questionnaire by Annett (*15*), required the subject to demonstrate hand preference on 12 unimanual tasks. Of the 42 subjects, 27 showed consistent right-hand preference and 15 showed mixed-hand preference, the latter group showing various combinations of right- and left-hand preferences (*16*). Consistent left-hand preference is rare, and no consistent left-handers were available in this sample. Clinical postmortem examinations were obtained and each whole brain was removed and immersion-fixed in buffered 10 percent Formalin (*17*). After fixation, the brain was bisected sagittally to expose the corpus callosum (*18*). On a photograph (Fig. 1), the line indicating the extent of the callosum was used to define anterior and posterior halves and a posterior fifth (*19*). The posterior fifth is roughly congruent with the splenium, which is difficult to define as it has no distinct anterior boundary. Total and partial area measurements of the callosum were made from tracings of the outline of the callosum from the photographs (at magnification $\times 1$) of the midsagittal section (*20*).

The right-handers (mean $\pm$ standard error of the mean, 50.3 $\pm$ 1.8 years old) and mixed-handers (48.7 $\pm$ 2.3 years) did not differ significantly in mean age at death [$t(40) = 0.51$, $P = 0.61$], nor in whole brain weight [1314 $\pm$ 20.6 g versus 1328 $\pm$ 43.3 g, respectively; $t(40) = 0.34$, $P = 0.74$] (*21*). The mixed-handers had significantly larger total, anterior half, and posterior half areas than the right-handers (Fig. 2). In contrast, the region of the posterior fifth did not differ significantly between hand groups (*22*).